The hydrodynamics of flagellar propulsion: helical waves

By J. J. L. HIGDON

Department of Applied Mathematics and Theoretical Physics, University of Cambridge†

The swimming of a micro-organism by the propagation of helical waves on a long slender flagellum is analysed. The model developed by Higdon (1979) is used to study the motion of an organism with a spherical cell body (radius A) propelled by a cylindrical flagellum (radius a, length L).

The average swimming speed and power consumption are calculated for helical waves (amplitude α, wavenumber k). A wide range of parameter values is considered to determine the optimal swimming motion. The optimal helical wave has $ak \approx 1$, corresponding to a pitch angle of 45°. The optimum number of waves on the flagellum increases as the flagellar length L/A increases, such that the optimum wavelength decreases as L/A increases. The efficiency is relatively insensitive to the flagellar radius a/A. The optimum flagellar length is $L/A \approx 10$.

The results are compared to calculations using two different forms of resistance coefficients. Gray–Hancock coefficients overestimate the swimming speed by approximately 20% and underestimate the power consumption by 50%. The coefficients suggested by Lighthill (1976) overestimate the swimming speed for large cell bodies ($L/A < 15$) by 20% and underestimate for small cell bodies ($L/A > 15$) by 10%. The Lighthill coefficients underestimate the power consumption up to 50% for $L/A < 10$, and overestimate up to 25% for $L/A > 10$. Overall, the Lighthill coefficients are superior to the Gray–Hancock coefficients in modelling swimming by helical waves.

1. Introduction

The swimming of micro-organisms by flagellar propulsion was analysed by Higdon (1979, henceforth referred to as I). In that paper, a method was presented for modelling the swimming of organisms employing general three-dimensional waves. The model was applied to organisms using planar waves to determine the effects of the parameters on the swimming speed and efficiency. In the present work, the model is applied to organisms employing three-dimensional waves; specifically, helical waves.

We consider an organism with a spherical cell body, radius A, propelled by a single flagellum, radius a, length L, which is attached to the cell body radially. A helical wave propagates along the flagellum with amplitude α and linear wavelength λ. The organisms to which this model apply include bacteria and eukaryotes. The major difference between these two groups is in the structure of the flagellum. The eukaryotic flagellum is an order of magnitude larger than the bacterial flagellum.

The hydrodynamic model as developed in I employs slender body theory for Stokes'

† Present address: Department of Chemical Engineering, Stanford University, California 94305.

flow. This allows the flagellum to be represented by distributions of stokeslets and dipoles along its centre-line. The sphere is represented by two sets of singularities. The first set consists of an image system which cancels the velocity on the sphere induced by the singularities along the flagellum. The second set is composed of the stokeslet, dipole and rotlet needed to match the velocity on the sphere due to translation and rotation.

The introduction of the singularities transforms the no-slip boundary condition into a set of singular integral equations for the singularity distributions. To solve these equations, the kernel is evaluated analytically over short intervals, and the results used to set up a system of linear algebraic equations. An iteration procedure is used to solve these equations numerically.

There have been several efforts to model the use of helical waves with resistance coefficients. Holwill & Burge (1963) examined helical waves in studying the locomotion of bacteria. Chwang & Wu (1971) considered helical waves for a wide variety of parameters covering many organisms. They introduced the concept of moment coefficients to calculate the moment due to rotation of the flagellum about its centre-line. Coakley & Holwill (1972) considered more general waves, including helical waves with elliptical cross-section and varying amplitude. In each of these studies, the force on the cell body was calculated using Stokes' drag formula, and the interaction of the cell body and flagellum was ignored. In addition, the flagellum and cell body were considered in isolation, avoiding consideration of the form of the junction between the two.

In the present work, the swimming motion is analysed to determine the effect of the parameters on the swimming speed and efficiency of the organism. The model is used to assess the accuracy of the resistance coefficient models and to determine the importance of the factors which have been ignored in previous models.

2. Velocity induced by singularity distributions

Applying slender body theory to the problem of flagellar propulsion, it was shown in I that the flagellum can be represented by distributions of stokeslets and dipoles along its centre-line. The errors in this approximation are order $O(a/L)$.

A stokeslet at the point $\mathbf{X}$ is defined by

$$S_{jk}(\mathbf{x}, \mathbf{X}) = \frac{\delta_{jk}}{r} + \frac{(x_j - X_j)(x_k - X_k)}{r^3}, \tag{1}$$

where

$$r = |\mathbf{x} - \mathbf{X}|.$$

A dipole at the point $\mathbf{X}$ is defined by

$$D_{jk}(\mathbf{x}, \mathbf{X}) = \frac{-\delta_{jk}}{r^3} + 3\frac{(x_j - X_j)(x_k - X_k)}{r^5}. \tag{2}$$

The velocity induced by distributions of stokeslets and dipoles along the flagellum is given by

$$u_j(\mathbf{x}) = \int_0^L \left[S_{jk}(\mathbf{x}, \mathbf{X}(s)) \frac{f_k(s)}{8\pi\mu} + D_{jk}(\mathbf{x}, \mathbf{X}(s)) \frac{d_k(s)}{4\pi} \right] ds, \tag{3}$$

where $\mathbf{f}$ and $\mathbf{d}$ are the stokeslet and dipole distributions and the integration extends along the flagellum.

It was shown in I that the dipole strength is determined by the component of stokeslet strength normal to the centre-line. In particular

$$d_k = -\frac{a^2}{4\mu} (\delta_{kl} - T_k T_l) f_l, \tag{4}$$

where $\mathbf{T}$ is the unit vector tangent to the flagellum, and a is the radius of the flagellum.

To account for the presence of the spherical cell body, the stokeslet S_{jk} in (3) must be replaced by the Green's function for the flow external to a sphere. This is accomplished by adding the terms which constitute the image system for the sphere.

The Green's function has the form:

$$G_{jk}(\mathbf{x}, \mathbf{X}) = S_{jk}(\mathbf{x}, \mathbf{X}) + S_{jk}^*(\mathbf{x}, \mathbf{X}), \tag{5}$$

where S_{jk} is the stokeslet and S_{jk}^* is the image system for the sphere. The exact expression for G_{jk} was derived by Oseen (1927) and is given in I, equation (3).

Adding the image system to (3), the expression for the induced velocity now has the form:

$$u_j(\mathbf{x}) = \int_0^L \left\{ [S_{jk}(\mathbf{x}, \mathbf{X}(s)) + S_{jk}^*(\mathbf{x}, \mathbf{X}(s))] \frac{f_k(s)}{8\pi\mu} + D_{jk}(\mathbf{x}, \mathbf{X}(s)) \frac{d_k(s)}{4\pi} \right\} ds. \tag{6}$$

This integral is evaluated by dividing the flagellum into N intervals in which $\mathbf{f}$ is assumed constant. The image system S_{jk}^* is singular inside the sphere, but well behaved along the flagellum. Thus, it may be integrated easily by numerical methods. The functions S_{jk} and D_{jk} are integrated analytically. Performing these operations and using (4) to eliminate $\mathbf{d}$, the induced velocity can be expressed in the form:

$$u_j(\mathbf{x}) = \sum_{n=1}^N \{ [K_{jk}(\mathbf{x}, \mathbf{X}(s_n)) + H_{jk}(\mathbf{x}, \mathbf{X}(s_n))] f_k(s_n) \}, \tag{7}$$

where $f_k(s_n)$ is the value of $\mathbf{f}$ in the nth interval, and $\mathbf{X}(s_n)$ is the midpoint of the nth interval. H_{jk} is the result of the numerical integration of the image system S_{jk}^*, and K_{jk} represents the terms integrated analytically. The exact expressions for H_{jk} and K_{jk} are given in I, equations (23) and (27) respectively.

The expression in equation (7) gives the velocity induced by the singularities along the flagellum and their images in the sphere.

3. Kinematics of flagellar motion

In this section, we consider the specification of the position and velocity of points on the flagellum when it assumes the form of a helical wave. A helical wave with constant amplitude α and wavenumber k is specified by:

$$(x, y, z) = (x, \alpha \cos (kx - \omega t), \alpha \sin (kx - \omega t)). \tag{8}$$

For the organisms under consideration, we have assumed that the flagellum is attached to the cell body radially. If this condition is to be satisfied with the wave (8), the centre of the cell body must be displaced from the helical axis (see figure 1 a). This situation occurs with a number of organisms; but in general, these have very irregular wave forms and are outside the class of organisms we wish to consider in this paper. To place the cell body on the helical axis, consider a slight modification of
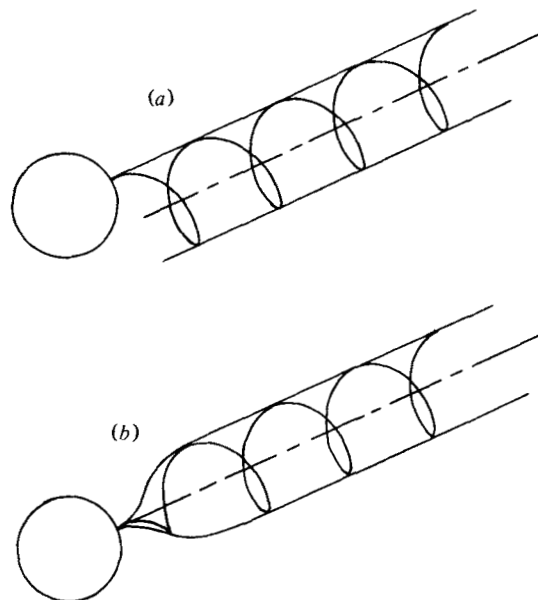
FIGURE 1. (*a*) Constant amplitude helical wave showing displacement of the cell body off the helical axis. (*b*) Modified wave with cell body centred on helical axis.

the helical wave. The wavenumber k remains constant, but the amplitude of the wave is modified by the function:

$$E(x) = [1 - \exp[-(k_E x)^2]]. \tag{9}$$

This function has the properties: $E(0) = 0$, $E'(0) = 0$ and $E(x)$ grows very rapidly to its asymptotic value, $E(\infty) = 1$.

The new helical wave is specified by

$$(x, y, z) = (x, E(x)\,\alpha\cos{(kx - \omega t)}, E(x)\,\alpha\sin{(kx - \omega t)}) \tag{10}$$

(see figure 1*b*).

Observe that the modified wave has a short 'end region' in which its amplitude increases rapidly, after which it is identical to the constant amplitude wave.

To obtain a co-ordinate system (X, Y, Z) consistent with the analysis of I, the origin is placed at the centre of the sphere with the X axis along the helical axis. The Y and Z axes are chosen such that the sphere does not rotate with respect to this frame. Call this co-ordinate system the body frame.

In the body frame, the flagellum is attached to the cell body at the point:

$$\mathbf{X}_0 = (X_0, 0, 0),$$

and the helical wave is expressed:

$$\mathbf{X}(X, t) = (X, E(X - X_0)\,\alpha\cos{(k(X - X_0) - \omega t)}, E(X - X_0)\,\alpha\sin{(k(X - X_0) - \omega t)}) \tag{11}$$
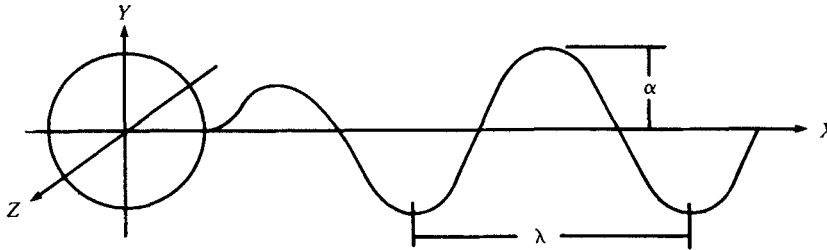
(see figure 2).

FIGURE 2. Wave form and co-ordinate system for locomotion by helical waves.

When the position of a point on an inextensible flagellum is given by $\mathbf{X}(s, t)$ where s is the arclength measured from $\mathbf{X_0}$, the velocity of the point is given by

$$\mathbf{u}(s, t) = \frac{\partial}{\partial t} \mathbf{X}(s, t). \tag{12}$$

The arclength s as a function of X and t is expressed as

$$s = \int_{X_0}^{X} \left[1 + \left(\frac{\partial Y(X, t)}{\partial X} \right)^2 + \left(\frac{\partial Z(X, t)}{\partial X} \right)^2 \right]^{\frac{1}{2}} dX. \tag{13}$$

Substituting from (11), we obtain:

$$s = \int_{X_0}^{X} [1 + (\alpha k E(X))^2 + (\alpha E'(X))^2]^{\frac{1}{2}} dX. \tag{14}$$

Note from this expression that s is a function of X only and is independent of t. Therefore,

$$\frac{\partial}{\partial t} \mathbf{X}(s, t) = \frac{\partial}{\partial t} \mathbf{X}(X, t). \tag{15}$$

Thus, the velocity of points on the centre-line of the flagellum is obtained by differentiating (11) with respect to t.

Differentiating (11) yields:

$$\mathbf{u}(X, t) = (0, \omega \alpha E(X - X_0) \sin (k(X - X_0) - \omega t), -\omega \alpha E(X - X_0) \cos (k(X - X_0) - \omega t)). \tag{16}$$

Note that this velocity may be written in the form:

$$\mathbf{u}(X, t) = (-\omega, 0, 0) \times (X, Y, Z), \tag{17}$$

where (X, Y, Z) is given by (11).

This shows that the helical wave formed by transverse bending waves on an inextensible flagellum is equivalent to the rotation of a rigid helix of the same form. The motion of the centre-line is identical; however, the velocity on the surface of the flagellum is different. The surface in the wave motion remains fixed with respect to its centre-line, while the surface of the rigid helix rotates about its centre-line.

At this point, it is convenient to define certain wave parameters not previously specified. The linear wavelength λ equals $2\pi/k$, and the linear wave speed V equals ω/k. The curvilinear wavelength Λ and wave speed c are not constants, due to the varying amplitude of the helical wave. Outside the special 'end region', they vary negligibly and their values are

$$\Lambda = \lambda[1 + \alpha^2 k^2]^{\frac{1}{2}} \quad \text{and} \quad c = V[1 + \alpha^2 k^2]^{\frac{1}{2}}. \tag{18}$$

The number of wavelengths N_λ is defined as the extension of the flagellum in the X direction divided by λ, the linear wavelength. The length of the flagellum is given by

$$L = \int_0^{\lambda N_\lambda} \{1 + [\alpha k E(x)]^2 + [\alpha E'(x)]^2\}^{\frac{1}{2}} \, dx. \qquad (19)$$

This completes the specification of the wave motion.

4. Boundary conditions

The no-slip boundary condition requires that the velocity of a point on the surface of the flagellum equal the velocity of the fluid at that point. The velocity of points on the flagellum with respect to the body frame is given by (17). The body frame is assumed to have velocity $\mathbf{U}_0$ and angular velocity $\boldsymbol{\Omega}_0$ with respect to the rest frame. Thus, the velocity of a point $\mathbf{X}$ on the flagellum with respect to the rest frame is expressed by

$$\mathbf{u}_R(\mathbf{X}) = \mathbf{U}_0 + \boldsymbol{\Omega}_0 \times \mathbf{X} + (-\omega, 0, 0) \times \mathbf{X}. \qquad (20)$$

The cell body has velocity $\mathbf{U}_0$ and angular velocity $\boldsymbol{\Omega}_0$ with respect to the rest frame. The singularities needed to match this velocity on the surface of the sphere are: a stokeslet and dipole for translation, and a rotlet for rotation. The velocity field produced by these singularities is

$$u_{H_j}(\mathbf{X}) = \tfrac{3}{4} A \left(S_{jk}(\mathbf{X}, 0) - \frac{A^2}{3} D_{jk}(\mathbf{X}, 0) \right) U_{0_k} + \frac{A^3}{|\mathbf{X}|^3} \epsilon_{jkl} X_l \Omega_{0_k} \qquad (21)$$

(see Happel & Brenner, 1965).

The boundary condition on the flagellum is now expressed by equating the velocity of the flagellum with the velocity induced by the singularities. This is expressed as

$$u_{R_j}(\mathbf{x}) = u_{H_j}(\mathbf{x}) + \sum_{n=1}^N \{[K_{jk}(\mathbf{x}, \mathbf{X}(s_n)) + H_{jk}(\mathbf{x}, \mathbf{X}(s_n))] f_k(s_n)\}, \qquad (22)$$

where $\mathbf{u}_R$ is the velocity of the flagellum, $\mathbf{u}_H$ is the induced velocity due to translation and rotation of the cell body, and the summation gives the velocity induced by the singularity distributions along the flagellum and their images as derived in § 2.

By evaluating this expression (22) at the N points: $\mathbf{X}(s_n)$, we obtain $3N$ equations in the $3N + 6$ unknowns: $\mathbf{f}(s_n)$, $\mathbf{U}_0$ and $\boldsymbol{\Omega}_0$.

The six additional equations come from the force and moment balances.

5. Force and moment balances

The organism is self propelled and is not influenced by any external forces. Therefore, the total force and moment on the organism are zero. As a stokeslet corresponds to a point force, the condition of zero force is equivalent to the total stokeslet strength being zero. To find the total stokeslet strength, we consider the contribution of the stokeslets along the flagellum, their images in the sphere and the stokeslet due to translation of the sphere. The stokeslet due to translation has strength $6\pi\mu A \mathbf{U}_0$. To find the strength of the images, consider the radial and transverse components of a stokeslet on the flagellum.

Let $\mathbf{F}$ be a stokeslet on the flagellum. Write $\mathbf{F}$ in the form

$$F_k = \left(F_j \frac{X_j X_k}{|\mathbf{X}|^2}\right) + \left(F_k - F_j \frac{X_j X_k}{|\mathbf{X}|^2}\right), \tag{23}$$

where the first bracket is the radial component and the second is the transverse component with respect to the sphere.

The strengths of the radial and transverse images were given in I, equations (7) and (8) respectively. Adding these image strengths, the total force on the organism due to the stokeslet $\mathbf{F}$ and its image is

$$F_k(1+C_T) + F_j\left(\frac{X_j X_k}{|\mathbf{X}|^2}\right)(C_R - C_T), \tag{24}$$

where

$$C_R = -\frac{3}{2}\frac{A}{|\mathbf{X}|} + \frac{1}{2}\frac{A^3}{|\mathbf{X}|^3}, \quad \text{and} \quad C_T = -\frac{3}{4}\frac{A}{|\mathbf{X}|} - \frac{1}{4}\frac{A^3}{|\mathbf{X}|^3}. \tag{25}$$

Summing over all stokeslets on the flagellum and adding the contribution due to translation of the sphere, the force balance yields

$$\sum_{n=1}^{N}\left\{\left[(1+C_T(s_n))\,\delta_{jk} + (C_R(s_n)-C_T(s_n))\frac{X_j X_k}{|\mathbf{X}|^2}\right]f_j(s_n)\,2\delta s_n\right\} + 6\pi\mu A U_{0_k} = 0, \tag{26}$$

where $2\delta s_n$ is the length of the nth interval.

For the moment balance, the contribution from the radial stokeslets is zero. The strength of the image rotlet in the sphere is given in I, equation (8). The moment about the centre of the sphere due to a stokeslet $\mathbf{F}$ at the point $\mathbf{X}$ and its image is

$$\epsilon_{ijk}X_j F_k\left(1 - \frac{A^3}{|\mathbf{X}|^3}\right). \tag{27}$$

The moment about the origin due to the rotation of the sphere is $8\pi\mu A^3\mathbf{\Omega}_0$.

Summing over all stokeslets on the flagellum, the moment balance becomes

$$\sum_{n=1}^{N}\left\{\left[\epsilon_{ijk}X_j f_k(s_n)\left(1 - \frac{A^3}{|\mathbf{X}|^3}\right)\right]2\delta s_n\right\} + 8\pi\mu A^3\Omega_{0_i} = 0. \tag{28}$$

6. Solution of equations

The complete set of equations is composed of the boundary condition (22), the force balance (26) and the moment balance (28). This is a set of $3N + 6$ equations for the $3N + 6$ unknowns: $\mathbf{f}(s_n)$, $\mathbf{U}_0$ and $\mathbf{\Omega}_0$. The solution of these equations is by an iteration procedure.

First, the boundary condition (22) is modified by making the following definitions:

$$Q_{jk}(s_m, s_n) = K_{jk}(\mathbf{X}(s_m), \mathbf{X}(s_n)) + H_{jk}(\mathbf{X}(s_m), \mathbf{X}(s_n)); \tag{29}$$

$$P_{jk}(s_m) = \sum_{n=1}^{N} Q_{jk}(s_m, s_n). \tag{30}$$

The boundary condition is now written as

$$u_{R_j}(s_m) = u_{H_j}(s_m) + P_{jk}(s_m)f_k(s_m) + \sum_{n=1}^{N}[f_k(s_n) - f_k(s_m)]\,Q_{jk}(s_m, s_n). \tag{31}$$

Equation (31) is multiplied by the inverse of P_{jk} and rearranged to obtain

$$f_i(s_m) = [P]_{ij}^{-1}(s_m)\left\{u_{R_j}(s_m) - u_{H_j}(s_m) - \sum_{n=1}^{N}[f_k(s_n) - f_k(s_m)]\,Q_{jk}(s_m, s_n)\right\}. \qquad (32)$$

This expression is used to define the iteration. The right-hand side of the equation depends on the previous values of **f**, while the left-hand side defines the next iteration. At each iteration, (32) is used to eliminate **f** from the force and moment balances, which are then solved simultaneously for $\mathbf{U_0}$ and $\mathbf{\Omega_0}$. The details of this procedure are described in I. Details of the computing are given in the appendix to this paper.

The solution of the system of equations defines the motion of the organism at a single instant of time. In general, the solution must be obtained at several instants in the cycle, and the quantities integrated to find the average swimming speed and power consumption. In the case of helical waves, we shall see that it is sufficient to evaluate at a single instant of time.

Consider a frame whose origin coincides with that of the body frame, but which rotates with angular velocity $(-\omega, 0, 0)$ with respect to the body frame. Call this the phase frame. In the phase frame, the flagellum appears stationary, while the cell body rotates with angular velocity $(\omega, 0, 0)$. Because the flagellum is stationary, and the cell body is spherical, the motion at any instant during the cycle is indistinguishable from any other instant. Therefore, the solution in the phase frame is independent of time.

The velocity of the phase frame with respect to the rest frame is $\mathbf{U_0}$, while the angular velocity of the phase frame with respect to the rest frame is:

$$\mathbf{\Omega}_p = (\Omega_{0_1} - \omega, \Omega_{0_2}, \Omega_{0_3}). \qquad (33)$$

The phase frame rotates with constant angular velocity $\mathbf{\Omega}_p$ with respect to the rest frame and translates with constant velocity $\mathbf{U_0}$, where $\mathbf{U_0}$ is referred to the phase frame. These conditions imply that the origin of the phase frame moves along a helical path with the helical axis parallel to the rotation vector $\mathbf{\Omega}_p$. Thus, the displacement of the cell body over a cycle is in the direction of $\mathbf{\Omega}_p$ and the average swimming speed is the component of $\mathbf{U_0}$ parallel to $\mathbf{\Omega}_p$. The average swimming speed is expressed:

$$\overline{U} = (\mathbf{U_0} . \mathbf{\Omega}_p)/|\mathbf{\Omega}_p|. \qquad (34)$$

The power consumption of the organism is obtained by integrating the product of the force and the velocity over the surface of the organism. This calculation may be performed with the velocity referred to any frame, because the total force and moment are zero. In the body frame, the velocity on the cell body is zero, and the power consumption may be calculated by summing the contributions along the flagellum.

Thus, the power is expressed as

$$P = \sum_{n=1}^{N}[\mathbf{f}(s_n) . \mathbf{u}(s_n)]\,2\delta s_n, \qquad (35)$$

where **u** is given by (17).

From the discussion of the phase frame and the fact that the power is independent of the frame, we conclude that the power is independent of time. Therefore, the average power consumption $\overline{P}$ is identically equal to the instantaneous power P defined by (35).

7. Results

In this section, we consider the effect of changes in the parameters on the swimming speed and power consumption of the organism. In particular, we wish to find the combination of parameters which leads to the optimal swimming motion. The optimal swimming motion is considered to be that which requires the minimum power to achieve a given swimming speed.

The organism consists of a spherical cell body, radius A, propelled by a single flagellum, radius a, length L. The flagellum forms a helical wave whose shape is specified by (11). The wave parameters are N_λ, αk and k/k_E.

The average swimming speed is considered in the non-dimensional form $\bar{U}/V$. The power consumption is non-dimensionalized as

$$\eta_0^{-1} = \bar{P}/6\pi\mu A \bar{U}^2. \tag{36}$$

The minimum value of η_0^{-1} defines the optimal swimming motion for the organism; hence, it is called the inverse efficiency.

The five parameters to be considered in evaluating the optimal motion are the wave parameters: N_λ, αk, k/k_E and the body parameters: a/A, L/A. First, we consider variation in the wave parameters for organisms with given body parameters. When the optimal wave form is found for each organism, we consider variation in the body parameters to determine the optimal configuration.

The swimming speed as a function of the number of waves N_λ, is shown in figure 3. In this figure, $\bar{U}/V$ is shown for three different length flagella with the parameters αk and k/k_E taking fixed values (which we shall see are their optimum values). In each case, the swimming speed rises rapidly to a maximum, and falls off gradually as N_λ increases past the maximum. To explain this behaviour, we consider the role of the cell body in the swimming motion.

As described in § 3, the helical wave is equivalent to the rotation of a rigid helix with angular velocity ω. This motion generates a torque on the organism which must be balanced by the counter rotation of the cell body with an angular velocity Ω. This counter rotation reduces the effective rotation rate of the helix to $\omega - \Omega$. The swimming speed is reduced proportionately.

As the number of waves on the flagellum is increased, while the wave remains geometrically similar, the amplitude and wavelength decrease. The torque on the flagellum is proportional to the length times the square of the amplitude of the wave. Therefore, increasing the number of waves reduces the torque by reducing the amplitude. This reduces Ω and hence increases the effective rotation rate of the helix. Thus, the swimming speed increases as the number of waves is increased.

The slow decay in swimming speed after the maximum has been reached is due to a different effect. The basis of flagellar propulsion is the fact that the resistance of a long slender body is much greater for normal motion than for tangential motion. As the thickness of the body increases, this effect is reduced. In the case of waves travelling on a flagellum, the significant parameter is the logarithm of the ratio of wavelength to flagellar diameter. As the wavelength decreases, this slenderness ratio decreases, and the mechanism becomes less effective.

The behaviour of the curves in figure 3 can now be explained. Consider first the case of the shortest flagellum, $L/A = 5$. The swimming speed reaches a maximum at
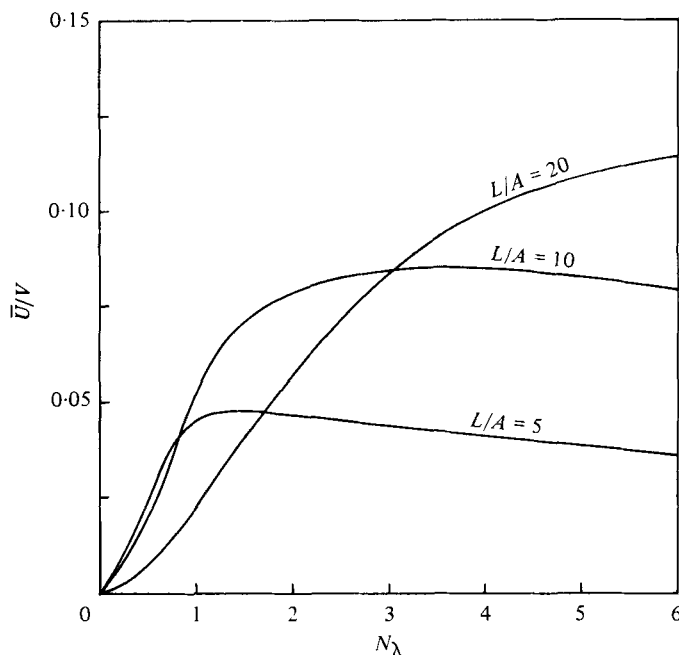
FIGURE 3. Average swimming speed as a function of number of waves. Curves are shown for three different length flagella with $a/A = 0.02$. Wave parameters: $\alpha k = 1$; $k/k_E = 1$.

$N_\lambda = 1$. At this point, the two mechanisms described above are balanced; that is, any further decrease in Ω will be at the cost of a reduction in the ratio of wavelength to diameter and will not increase the swimming speed. For the case $L/A = 10$, the maximum swimming speed is reached at $N_\lambda = 3$. As the flagellum is longer in this case, the cell body is less effective in providing a balancing torque, and the amplitude of the wave must be decreased by splitting the flagellum into a larger number of waves. Also, the longer length of the flagellum means that more waves may be employed before the ratio of wavelength to diameter becomes too small. This trend is further demonstrated in the case $L/A = 20$, for which the maximum swimming speed occurs at a value of $N_\lambda > 6$.

The power consumption as a function of N_λ is shown in figure 4. The first point to notice is that the optimal swimming motion does not occur at the same point as the maximum swimming speed, but at a value of N_λ at which the swimming speed begins to level off. The optimal values of N_λ in the three cases are: $N_\lambda = 1$ for $L/A = 5$; $N_\lambda = 1.5$ for $L/A = 10$; and $N_\lambda = 4.5$ for $L/A = 20$.

In examining the behaviour of η_0^{-1} in figure 4, we return to the role of the cell body in the swimming motion. The power required to rotate the cell body is quite large compared to the power required for the flagellum. Thus, it is essential to reduce the rotation rate of the cell body. Increasing the number of waves decreases the rotation rate, and hence decreases the power consumption. At the same time, it increases the swimming speed, leading to a further reduction in η_0^{-1}.

We noted above that the propulsive mechanism relies on the fact that the normal forces are much larger than the tangential forces. As the slenderness ratio is reduced, the ratio of the normal force to the tangential force decreases. The resultant decrease
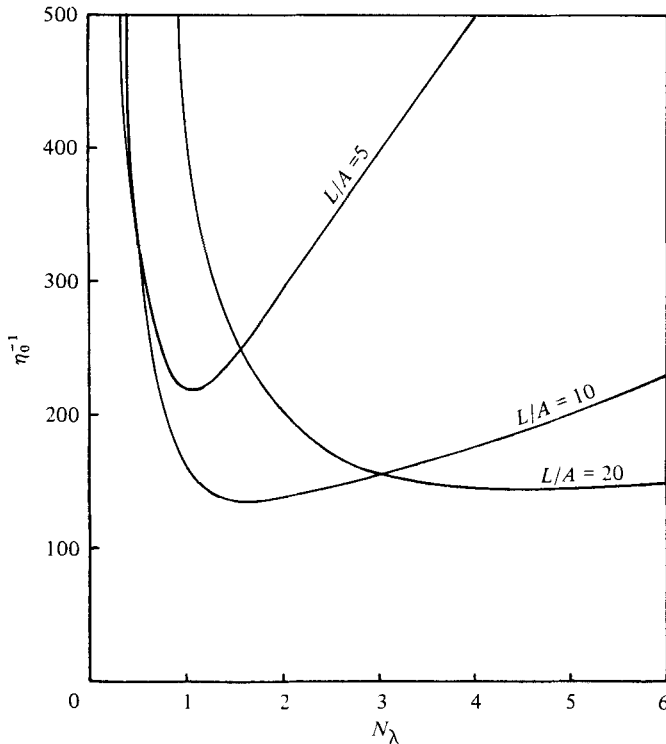
FIGURE 4. Power consumption in the non-dimensional form (36) as a function of number of waves. Curves are shown for three different length flagella with radius $a/A = 0.02$. Wave parameters: $\alpha k = 1$; $k/k_E = 1$.

in swimming speed causes an increase in η_0^{-1}. In addition, the magnitude of both force components increases when the slenderness ratio is decreased. This produces a further increase in η_0^{-1}.

A third effect which becomes important when the number of wavelengths grows large is the interference between neighbouring waves. When the waves are too close together, the velocity induced by one segment acts on its neighbours to increase the drag on the flagellum. This factor, together with the increase in the magnitude of the forces, causes the optimal value of N_λ to be reached before the swimming speed reaches its maximum. The optimal value is reached when the increase in swimming speed is insufficient to offset the increase in power consumption.

The power consumption as a function of αk is shown in figure 5 for three different length flagella. In each case, the optimum value is approximately $\alpha k = 1$. This corresponds to a segment of the flagellum making an angle of 45° with the helical axis. For values of $\alpha k < 1$, the reduced angle means that each segment of the flagellum contributes a smaller thrust per unit length. The low swimming speed which results contributes to a higher η_0^{-1}. For large values of αk, the increased power consumption is due to a combination of factors. The increased amplitude increases the torque causing the cell body to rotate faster. As stated above, this requires a large power expenditure and decreases the efficiency. In addition, increasing αk, while holding the other wave parameters constant, reduces the wavelength. This brings neighbouring
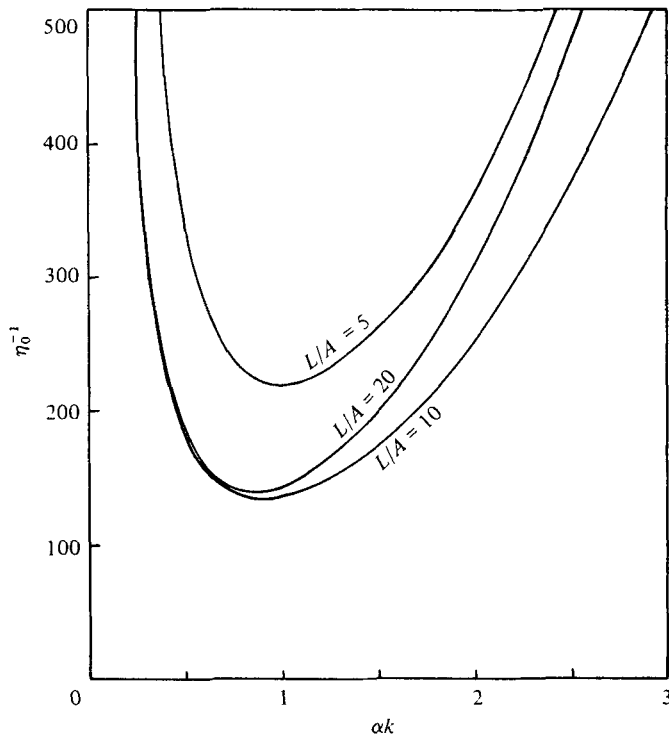
FIGURE 5. Power consumption (36) as a function of αk. Curves are for three different length flagella with radius $a/A = 0.02$. Wave parameters: optimum N_λ, $k/k_E = 1$.

waves closer together and decreases the efficiency due to interference between the waves.

The swimming speed as a function of αk is shown in figure 6. The swimming speed reaches its maximum value at $\alpha k = 2$. For the organisms with shorter flagella ($L/A = 5, 10$), the swimming speed remains constant at larger values of αk; while the swimming speed of the organism with the longest flagellum ($L/A = 20$) decreases slightly for $\alpha k > 2$. We note that the maximum swimming speed occurs at a much greater angle than the angle for the optimal swimming motion. The optimum value of αk is the value for which an increase in swimming speed is just offset by the increase in power consumption. If αk increases further, the swimming speed continues to increase, but at an ever greater energetic cost. This explains why the maximum swimming speed occurs at a larger αk than the optimal motion.

The final wave parameter to be considered is k/k_E. This parameter is a measure of how quickly (i.e. over what distance) the helical wave reaches its full amplitude – starting at zero amplitude at the point of contact with the cell body. The smaller k/k_E, the more rapidly the amplitude increases to its maximum value. For example, a value $k/k_E = 1$ means that the wave reaches 90% of its maximum amplitude in the first quarter wavelength. For $k/k_E = 2$, the wave reaches 50% of its maximum in the first quarter wavelength.

Figure 7 shows the dependence of η_0^{-1} on k/k_E. For the case: $L/A = 20$, $N_\lambda = 4.5$, the power consumption varies negligibly over the values of k/k_E considered. For $L/A = 10$, $N_\lambda = 1.5$, the power consumption remains virtually unchanged up to
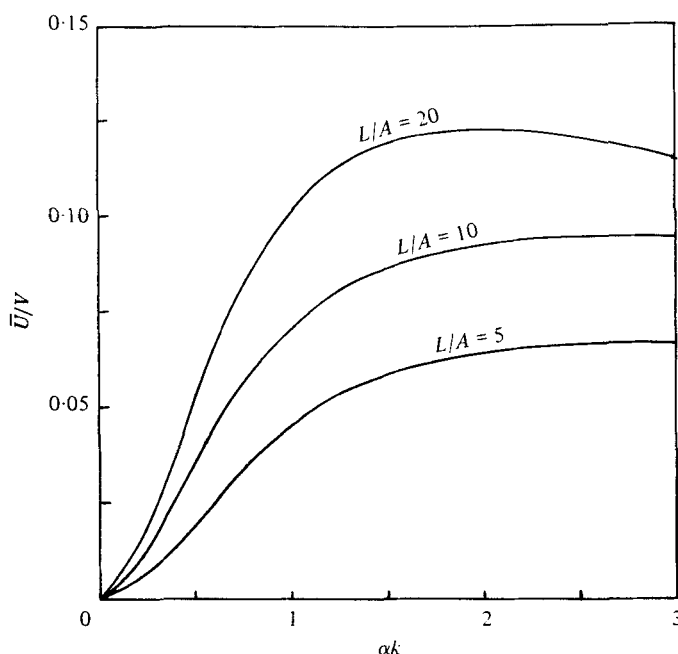
FIGURE 6. Average swimming speed as a function of αk. Curves are for three different length flagella with radius $a/A = 0.02$. Wave parameters: optimum N_λ; $k/k_E = 1$.

$k/k_E = 5$, after which it increases rapidly. Similarly, for $L/A = 5$, $N_\lambda = 1$, the power is unchanged up to $k/k_E = 3$ and then increases rapidly. The rapid increase in power in these two cases reflects the fact that, for the respective values of k/k_E, the wave is far below its optimal amplitude over a major portion of the flagellum. We conclude that the value of k/k_E does not affect the efficiency of the swimming motion, except in circumstances where the 'end region' occupies a substantial fraction of the flagellar length.

In summary, we find that the optimal helical wave form has $\alpha k = 1$, and that the optimum number of waves depends on the length of the flagellum. In general, the optimum number of waves increases faster than the length of the flagellum. Thus, the optimal wavelength decreases slowly as the flagellar length increases. The parameter k/k_E does not have an optimal value, but must be small enough for the wave to reach full amplitude within a small fraction of its length.

We turn our attention to consideration of the body parameters a/A and L/A. Figure 8 shows power consumption η_0^{-1} as a function of a/A. All three organisms show a slight increase in η_0^{-1} as the flagellar radius increases. The primary cause of this increase is that the cell body is less able to resist the torque of the thicker flagellum, and hence has a higher rotation rate and power consumption. In addition, the increased radius of the flagellum decreases the slenderness ratio, making the swimming motion less efficient. This effect is slight, as it depends on the ratio of the normal to tangential forces, whereas the increased rotation rate of the sphere results from the increased magnitude of the forces. The increase in power consumption is largest for the organism with the longest flagellum ($L/A = 20$), because it is the least able to resist the torque generated on the flagellum.
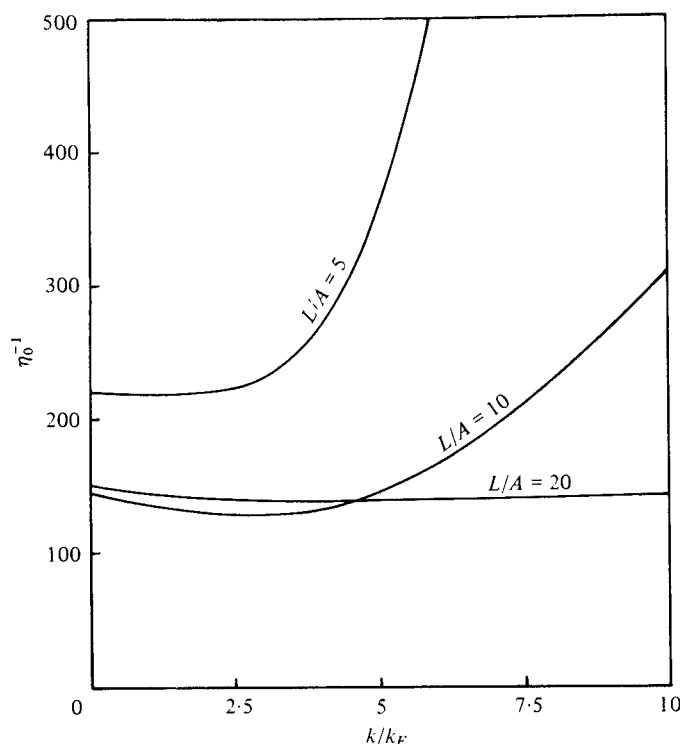
FIGURE 7. Power consumption (36) as a function of k/k_E. Curves are for three different length flagella with radius $a/A = 0.02$. Wave parameters: optimum N_λ and αk.

The swimming speed as a function of a/A is shown in figure 9. The speed varies negligibly for $L/A = 5$ and $L/A = 10$, because the slight increase in thrust due to the thicker flagellum is offset by the reduced effective rotation rate of the helix. The rotation rate is reduced, because the increased torque on the flagellum increases the counter rotation of the cell body. The swimming speed for $L/A = 20$ decreases slightly with increasing flagellar radius, because the cell body is less effective at countering the torque in this case.

It is interesting to compare the results of figure 9 with the conclusions of Chwang & Wu (1971) who found that the swimming speed $\overline{U}/V$ reached a maximum for a/A in the range $0.02 < a/A < 0.07$. In figure 9, we see very little variation in this range and no maximum value. The explanation for this disparity is that Chwang & Wu plotted the curves holding L/a constant, while the curves in figure 9 have L/A constant.

To examine this problem further, we look at the swimming speed as a function of L/A holding a/A constant (figure 10). The curves show that the swimming speed increases rapidly as the length of the flagellum increases, levelling off near $L/A = 20$. For the small values of L/A, the flagellum is too short to effectively propel the organism. This is due to interference with the cell body, which is proportionately more important for a short flagellum than for a long one. For very long flagella, the extra thrust generated by the extra length is negated by the reduced effective rotation rate of the helix. Once again, this is due to the increased torque on the flagellum.

By considering the dependence of $\overline{U}/V$ on a/A and L/A separately, we can deter-
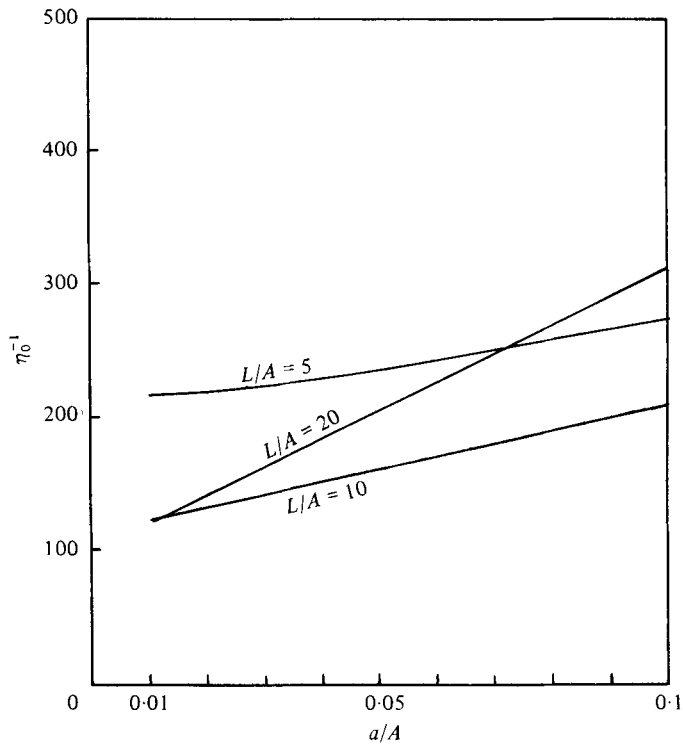
FIGURE 8. Power consumption (36) as a function of flagellar radius, a/A, for three different length flagella. Wave parameters: optimum N_λ, αk and k/k_E.
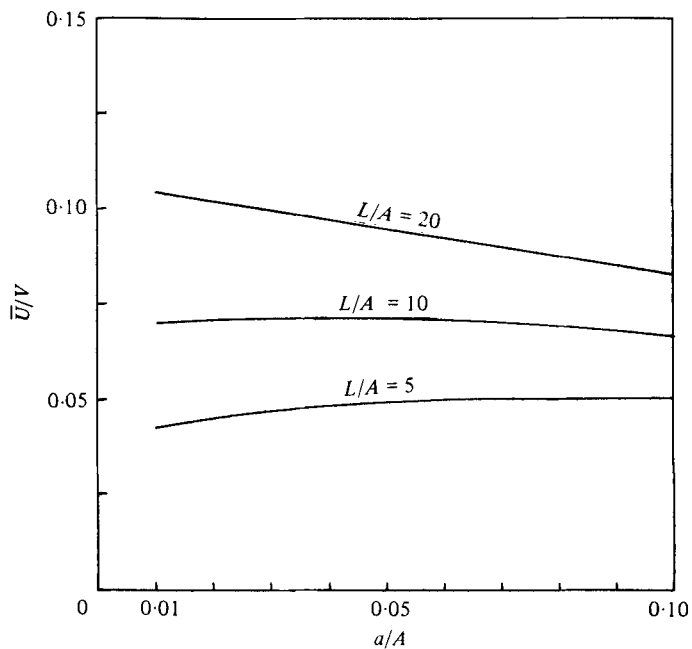

FIGURE 9. Average swimming speed as a function of flagellar radius a/A, for three different length flagella. Wave parameters: optimum N_λ, αk and k/k_E.

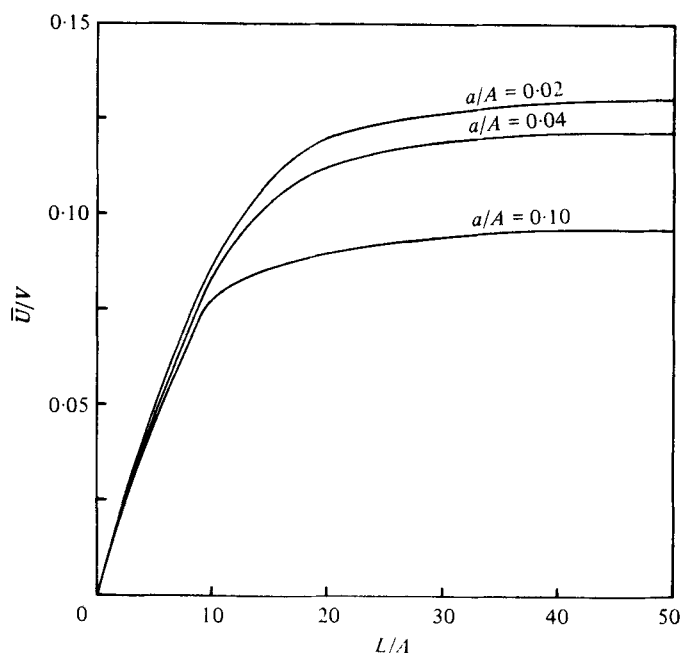FIGURE 10. Average swimming speed as a function of flagellar length L/A for three different flagellar radii. Wave parameters: optimum αk and k/k_E. N_λ equals value for maximum swimming speed $\overline{U}/V$.

mine how a maximum swimming speed is achieved. The first point to note from figures 9 and 10 is that a maximum swimming speed is not found for either a/A or L/A independently. We find that the maximum swimming speed depends on a combination of the parameters. If we allow a/A and L/A to increase together as Chwang & Wu did, we find that, for low values of the parameters, the swimming speed increases as the parameters increase, just as the swimming speed increases for increasing *length* in figure 10. For larger values, the swimming speed decreases as the parameters increase, as seen for the curve $L/A = 20$ in figure 9, in which $\overline{U}/V$ decreases for increasing *radius*. Thus, by allowing the parameters a/A and L/A to increase concurrently, a maximum swimming speed is found. Although the maximum depends on the values of both parameters, a comparison of figures 9 and 10 shows that the swimming speed is more sensitive to changes in the flagellar length than to changes in its radius.

The question of maximum swimming speed and its dependence on the parameters is very interesting, but it is not as important from a biological standpoint as the determination of the optimal swimming motion. The power consumption as a function of flagellar length L/A is shown in figure 11. In contrast to the result for maximum swimming speed, there is a clear minimum in the power consumption as a function of flagellar length. The optimal length is $L/A = 10$ when the radius is $a/A = 0.10$ and $L/A \approx 12$ when the radius is in the range: $0.02 < a/A < 0.04$. When the flagellum is shorter than the optimum length, it is less effective at propelling the organism due to its proximity to the cell body. The interference with the cell body reduces the swimming speed and increases the power consumption. When the flagellum is longer
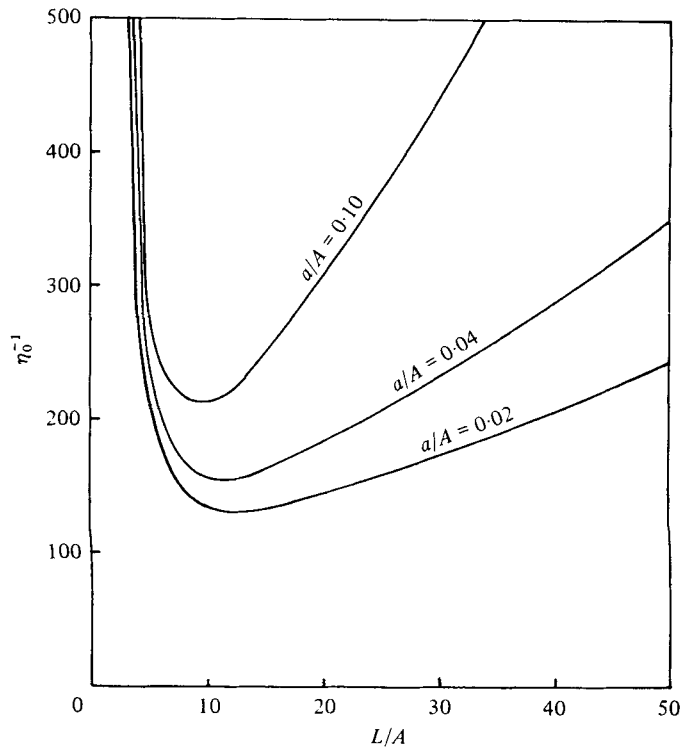
FIGURE 11. Power consumption (36) as a function of flagellar length L/A for three different flagellar radii. Wave parameters: optimum N_λ, αk and k/k_E.

than the optimum length, it requires more power, while producing only a marginal increase in swimming speed. This reduces the efficiency.

It is interesting to note that the optimum flagellar length is much shorter for helical waves than for the plane waves examined in I. This result may be explained by the fact that all segments of the helix contribute to the thrust, while for plane waves, some segments produce drag only. This result corresponds to the situation found among actual organisms, in which the organisms with shorter flagella employ helical waves, while those with longer flagella employ plane waves. There are, of course, exceptions to this rule, including many organisms whose wave form changes from planar to helical as it travels along the flagellum.

In summary, we find that the optimum flagellar length is approximately $L/A = 10$. The power consumption varies slowly with flagellar radius, decreasing as a/A decreases over the range of physically realistic radii. The swimming speed of the organism increases monotonically with increasing L/A and decreases monotonically with increasing radius a/A. If the ratio of the two parameters is held constant, a maximum swimming speed is found which depends on the ratio L/a.
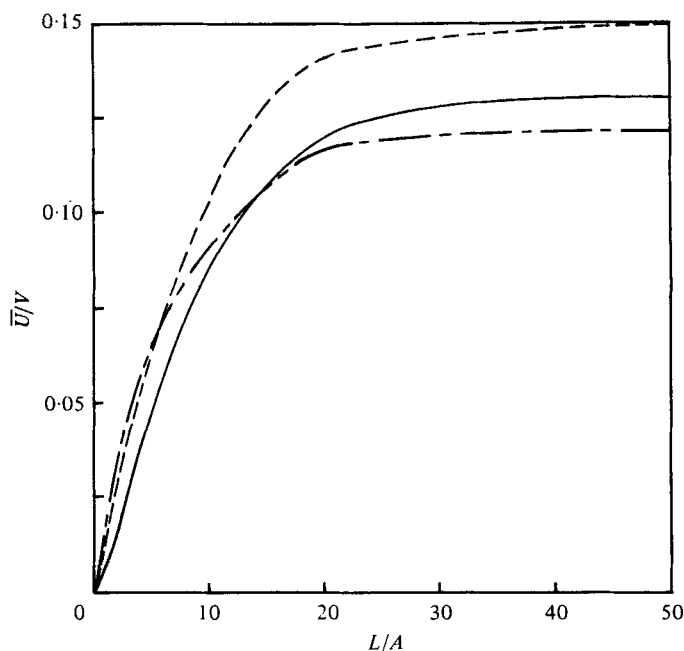
FIGURE 12. Average swimming speed as a function of flagellar length, L/A, showing difference between exact calculation and two resistance coefficient models. Flagellar radius $a/A = 0.02$. Wave parameters: optimum N_λ, αk and k/k_E. ——, exact; ———, Gray–Hancock; —·—, Lighthill.

8. Effectiveness of resistance coefficients

To evaluate the validity of previous models, we consider the accuracy of two resistance coefficient models in estimating the swimming speed and power consumption of an organism. The simplest form of resistance coefficient which has long been used by workers in the field is based on the asymptotic results obtained by Hancock (1953). These coefficients were first used by Gray & Hancock (1955) and have proved quite accurate in determining the swimming speed of organisms using plane waves (see I, §10). The Gray–Hancock coefficients are of the form:

$$K_T = \frac{2\pi\mu}{\ln[2\lambda/a]-0.5} \quad \text{and} \quad K_N = \frac{4\pi\mu}{\ln[2\lambda/a]+0.5}, \tag{37}$$

where λ is the linear wavelength.

Lighthill (1976) analysed the use of helical waves and obtained an exact solution for the swimming speed and power consumption of an infinite helical wave. He used this result to formulate improved resistance coefficients. First, he specified tangential and normal coefficients to be used to calculate the zero thrust part of the force distribution. These coefficients are expressed as

$$K_T = \frac{2\pi\mu}{\ln[2q/a]} \quad \text{and} \quad K_N = \frac{4\pi\mu}{\ln[2q/a]+0.5}, \tag{38}$$

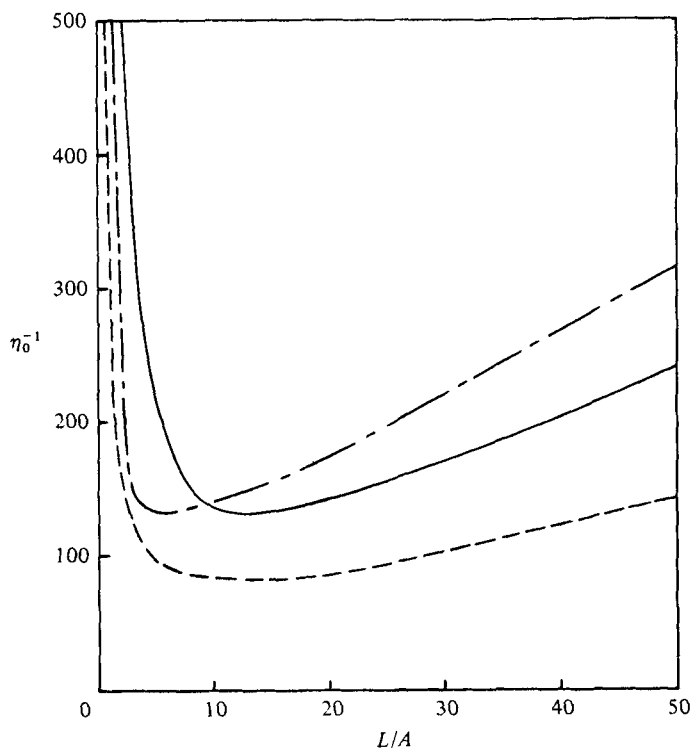where Λ is the curvilinear wavelength and $q = 0.09\Lambda$.

FIGURE 13. Power consumption (36) as a function of flagellar length, L/A, showing difference between exact calculation and two resistance coefficient models. Flagellar radius $a/A = 0.02$. Wave parameters: optimum N_λ, αk and k/k_E. ——, exact; ———, Gray–Hancock; —·—, Lighthill.

In calculating the component of force which generates a net thrust, he suggested that the force could be crudely estimated by a single coefficient giving thrust per unit length divided by velocity. The thrust coefficient has the form:

$$K_X = \frac{2\pi\mu}{\ln\left[2q_X/a\right]}. \tag{39}$$

The parameter q_X depends on the values of the wave parameters. For a graphical specification of q_X and a complete discussion of the model, see Lighthill (1976, pp. 213–221).

Figure 12 shows the swimming speed as a function of flagellar length, as calculated by the method of this paper and by the two resistance coefficient models. Both resistance coefficient models overestimate the swimming speed for short flagella ($L/A < 15$). This is due, in part, to the fact that these models do not consider the interference of the cell body. The Gray–Hancock model continues to overestimate the swimming speed by approximately 20 % over the entire range of lengths considered. The Lighthill model underestimates the swimming speed for organisms with $L/A > 15$, but is within 10 % of the actual swimming speed over the entire range of L/A. It is interesting to note that the Lighthill model is most accurate over the range $10 < L/A < 20$, a range in which a large number of actual organisms are found.

The power consumption η_0^{-1} as a function of flagellar length is shown in figure 13. The Gray–Hancock model underestimates the power consumption over the range of L/A by approximately 50 %. The Lighthill model underestimates the power for $L/A < 10$ and overestimates for $L/A > 10$. The underestimate for short flagella is rather extreme, due to the failure to account for the interference with the cell body. A second problem is that shorter flagella employ fewer wavelengths, making the assumptions of the Lighthill model less valid. The overestimate for $L/A > 10$ is approximately 25 %. Once again, the Lighthill model is most accurate over the range of L/A in which many actual organisms are found.

The overall conclusion is that resistance coefficients can given an accurate estimate for the swimming speed, but are unsuccessful in estimating the power consumption, especially for organisms with relatively short flagella (or alternatively, large cell bodies) $-L/A \approx 5$. As this length is characteristic of protozoa, it may be regarded as a serious failure of resistance coefficient models. Finally, we note that for helical waves, the Lighthill model is clearly superior to the Gray–Hancock model.

Appendix. Computing

The numerical procedures employed in this paper divide the flagellum into N segments. All segments were of equal length with the exception of the segments at the ends, which were chosen to be not less than twice the diameter of the flagellum. All calculations were performed using IBM 370 double precision to avoid errors in dealing with large numbers whose difference is very small. The large matrices were stored as single precision to save storage space.

The iteration procedure converged with an error of less than 1 % in the swimming speed and power consumption after four iterations. The iteration was carried further to ascertain that this was a true convergence.

The number of segments required varies according to the values of the wave parameters, but for a typical case, 20 segments per wavelength produces an error of less than 1 %.

For a general three-dimensional wave with the flagellum divided into 40 segments, the calculations required approximately 8 s of CPU time on the IBM 370.

To test the accuracy of the image system, the velocity was evaluated at points on the boundary. The exact expression for the Green's function was compared with its far field expansion, and the Cartesian expression was checked against the simpler result for the radial component.

To test the accuracy of the solution, the calculated velocity was compared with the velocity of the flagellum at points along the flagellum. Comparisons were made with asymptotic theories based on force coefficients with calculations done both analytically and numerically.

REFERENCES

CHWANG, A. T. & WU, T. Y. 1971 *Proc. Roy. Soc.* B **178**, 327.

COAKLEY, C. J. & HOLWILL, M. E. J. 1972 *J. Theor. Biol.* **35**, 525.

GRAY, J. & HANCOCK, G. J. 1955 *J. Exp. Biol.* **32**, 802.

HANCOCK, G. J. 1953 *Proc. Roy. Soc.* A **217**, 96.

HAPPEL, J. & BRENNER, H. 1965 *Low Reynolds Number Hydrodynamics*. Philadelphia: SIAM.

HIGDON, J. J. L. 1979 *J. Fluid Mech.* **94**, 305.

HOLWILL, M. E. J. & BURGE, R. E. 1963 *Arch. Biochem. Biophys.* **101**, 249.

LIGHTHILL, M. J. 1976 *SIAM Reviews* **18**, 161.

OSEEN, C. W. 1927 *Hydrodynamik*. Leipzig: Akad. Verlag.